Climate Dynamics
https://doi.org/10.1007/s00382-019-04980-1

A bias-corrected projection for the changes in East Asian summer monsoon rainfall under global warming

Shijie Zhou[1,3] · **Gang Huang**[1,2,3,5] · **Ping Huang**[1,4,5]

Received: 6 November 2018 / Accepted: 9 September 2019

Abstract

Projecting regional rainfall changes in a warmer climate attracts ongoing attention. However, large uncertainty still exists in multi-model projection. In this study, we introduce a bias-corrected method to correct the multi-model projection of changes in East Asian summer monsoon (EASM) rainfall based on the historical and RCP8.5 runs of 25 models from phase 5 of Coupled Model Intercomparison Project. Firstly, the total rainfall changes are separated into the thermodynamic component due to increased specific humidity and the dynamic component due to circulation changes. The thermodynamic component is corrected using the observed present-day rainfall and the increase rate of specific humidity based on the wet-get-wetter mechanism. On the other hand, the dynamic component with the circulation changes is corrected based on a "spatial emergent constraint" method, which is further validated by the perfect model approach. Together, these corrections give an integrated projection for EASM rainfall changes under global warming. Such an approach can improve the signal-to-noise ratio of projection effectively, from the original 0.73 of the multimodel mean to around 1.9. The corrected projection of EASM rainfall changes shows a pronounced increase in southern China, the northwest Pacific and a belt from northern China to northeastern China, and a weak increase in other EASM regions.

Keywords East Asian summer monsoon · Rainfall · Bias correction · CMIP5 · Global warming

1 Introduction

Precipitation is sensitive to climate change (Wu et al. 2013). Under global warming, global average precipitation is likely to increase by 1–3% $°C^{-1}$ over the 21st century (Held and Soden 2006). On regional scales, considerable uncertainties still exist in precipitation projections, reflected by large spread among the models from phase 5 of the Coupled Model Intercomparison Project (CMIP5) (Kent et al. 2015). Unreliable regional rainfall projection is an ongoing problem. Improving our comprehension of the underlying physical processes, as well as reducing model biases, will improve the confidence of regional projections (Xie et al. 2015).

East Asian summer monsoon (EASM), as an independent component in the Asian monsoon system, contributes nearly half of the annual precipitation in China (Ding and Chan 2005; de Carvalho 2016). Climate models project a robust increase in EASM rainfall due to global warming (Ueda et al. 2006; Hsu et al. 2012; Chen and Sun 2013; Kitoh et al. 2013; Kusunoki and Mizuta 2013; Seo et al. 2013; Endo and Kitoh 2014; Wang et al. 2014). Previous studies proposed several mechanisms for the changes in the large-scale

Electronic supplementary material The online version of this article (https://doi.org/10.1007/s00382-019-04980-1) contains supplementary material, which is available to authorized users.

✉ Gang Huang
hg@mail.iap.ac.cn

✉ Ping Huang
huangping@mail.iap.ac.cn

[1] State Key Laboratory of Numerical Modeling for Atmospheric Sciences and Geophysical Fluid Dynamics, Institute of Atmospheric Physics, Chinese Academy of Sciences, Beijing 100029, China

[2] Laboratory for Regional Oceanography and Numerical Modeling, Qingdao National Laboratory for Marine Science and Technology, Qingdao 266237, China

[3] University of Chinese Academy of Sciences, Beijing 100049, China

[4] Center for Monsoon System Research, Institute of Atmospheric Physics, Chinese Academy of Sciences, Beijing 100190, China

[5] Joint Center for Global Change Studies (JCGCS), Beijing 100875, China

Published online: 13 September 2019

hydrological cycle under global warming. For example, the wet-get-wetter mechanism named the thermodynamic effect emphasizes the increases in low-tropospheric water vapor under global warming, increasing rainfall in convection zones (Chou and Neelin 2004; Held and Soden 2006). However, such increased levels of global mean rainfall at a rate of 1–3% $°C^{-1}$ will be limited by the simultaneous increase in radiative energy, which is lower than the rate of enhanced specific humidity at nearly 7% $°C^{-1}$ (e.g., Allen and Ingram 2002). These different rates of change should lead to a slowdown in atmospheric circulation (Vecchi et al. 2006), which in turn will partially offset the increased rainfall induced by moister conditions. Another important process, the warmer-get-wetter mechanism suggests that tropical rainfall changes are correlated with the spatial variation of sea surface temperature (SST) warming, because the moist stability change is dominated by the SST warming pattern in the tropics (Xie et al. 2010; Huang et al. 2013; Huang 2014).

Moreover, for the regional precipitation changes over land, more processes related to the relative humidity and land-sea temperature contrasts are important factors, which complements the "wet-get-wetter" mechanism for the thermodynamic component (Byrne and O'Gorman 2013; Roderick et al. 2014; Byrne and O'Gorman 2015).

Moisture budget decomposition is a widely used method in studies of precipitation changes (Chou et al. 2009; Seager et al. 2010; Huang et al. 2013; Endo and Kitoh 2014; Huang 2014; Brown et al. 2016; Li and Ting 2017; Zhou et al. 2018). Zhou et al. (2018) suggested that the EASM rainfall changes can be divided into a thermodynamic component due to moisture increase and a dynamic component due to changes in circulation by employing a simplified moisture budget decomposition from Huang et al. (2013). The thermodynamic component related to moisture increase is proportional to the local moisture increase rate and the historical rainfall climatology (Chou et al. 2009, 2013). This result implies that we can use the observed rainfall climatology to replace the modelled historical rainfall climatology in the thermodynamic component to limit the intermodel spread of rainfall climatology among the models.

On the other hand, the EASM circulation changes in the dynamic component of rainfall changes shows large intermodel discrepancies (Mike et al. 1994; Hu et al. 2003; Kimoto 2005; Li and Ting 2017), although the skill of simulating EASM circulation is constantly improving (Sperber et al. 2013; Song and Zhou 2014; Gao et al. 2015). For long-term projections, the intermodel uncertainty is the dominant source of uncertainty in projections compared with the internal variability and scenario uncertainty (Hawkins and Sutton 2009, 2011). Although the multimodel mean (MMM) is credited with improving the reliability of projections (Thomson et al. 2006; Knutti 2010; Collins et al. 2012), the possible common model biases could affect the projections of future climate change in MMM (Zheng et al. 2011; Li and Xie 2014). In recent years, the "emergent constraint" concept, which rely on intermodel relationships between the current climate and future change among the models, has been widely used to constrain the intermodel discrepancies in the future climate change (Bracegirdle and Stephenson 2012, 2013; Cox et al. 2013; Klein and Hall 2015; Hall et al. 2019). Huang and Ying (2015) extended the original constraint for regional mean to a spatial emergent constraint with a linear ensemble pattern regression method to correct regional climate changes projected by MMM. The spatial emergent constraint strategy with the ensemble pattern regression method establishes the historical–future relationships to correct the common change bias linked with the common historical bias. It has been shown to efficiently improve the robustness when applied to the projection of the tropical Pacific SST warming pattern (Huang and Ying 2015) and could be practicable for the EASM circulation changes with apparent spatial pattern.

This paper describes a bias-corrected method to correct the changes in EASM precipitation under global warming projected by CMIP5 models. First, we divide the total rainfall change into thermodynamic and dynamic components by adopting the moisture budget decomposition, which has been demonstrated to be appropriate in the EASM regions in the previous study (Zhou et al. 2018). For the thermodynamic component, we use the Clausius–Clapeyron scaling based on the wet-get-wetter mechanism (Held and Soden 2006) to calculate the rainfall change induced by the increased water vapor and use it to replace the thermodynamic component. For the dynamic component, we use the spatial emergent constraint with the ensemble pattern regression method to reduce the uncertainty induced by the common historical simulation bias. The perfect model approach is performed to validate the method used in the dynamic correction. Then, we examine the corrected projection of EASM rainfall changes under future global warming of 1.5 °C and 2 °C relative to pre-industrial levels. The models and data used in our study are presented in Sect. 2. Details of the correction method are provided in Sect. 3. Section 4 reports the consequences of the corrections. Finally, conclusions and some further discussion are given in Sect. 5.

2 Models and data

We use the outputs of 25 models from the historical run and Representative Concentration Pathway (RCP) 8.5 run from CMIP5. Details of the 25 models are listed in Table 1. The long-term mean at the end of the 20th century (1981–2000) and the 21st century (2079–2098) represent the historical climatology and the future climatology, respectively. Their difference is defined in this study as the

Table 1 List of the 25 CMIP5 models used in this study

Model	Institute	Resolution (Lon × Lat, levels)
ACCESS1.0	CSIRO (Commonwealth Scientific and Industrial Research Organisation, Australia), and BOM (Bureau of Meteorology, Australia)	192 × 145, L38
ACCESS1.3		192 × 145, L38
BCC-CSM1.1	Beijing Climate Center, China Meteorological Administration	128 × 64, L26
BNU-ESM	College of Global Change and Earth System Science, Beijing Normal University	128 × 64, L26
CanESM2	Canadian Centre for Climate Modelling and Analysis	128 × 64, L35
CCSM4	National Center for Atmospheric Research	288 × 192, L27
CESM1(BGC)	National Science Foundation, Department of Energy, National Center for Atmospheric Research	288 × 192, L27
CESM1(CAM5)		288 × 192, L27
CNRM-CM5	Centre National de Recherches Meteorologiques/Centre Europeen de Recherche et Formation Avancees en Calcul Scientifique	256 × 128, L31
CSIRO Mk3.6.0	Commonwealth Scientific and Industrial Research Organisation in collaboration with the Queensland Climate Change Centre of Excellence	192 × 96, L18
GFDL CM3	Geophysical Fluid Dynamics Laboratory	144 × 90, L48
GFDL-ESM2G		144 × 90, L24
GFDL-ESM2M		144 × 90, L24
GISS-E2-H	NASA Goddard Institute for Space Studies	144 × 90, L40
GISS-E2-R		144 × 90, L40
HadGEM2-ES	Met Office Hadley Centre	192 × 145, L38
IPSL-CM5A-LR	Institut Pierre-Simon Laplace	96 × 96, L39
IPSL-CM5A-MR		144 × 143, L39
IPSL-CM5B-LR		96 × 96, L39
MIROC5	Atmosphere and Ocean Research Institute (The University of Tokyo), National Institute for Environmental Studies, and Japan Agency for Marine-Earth Science and Technology	256 × 128, L40
MIROC-ESM	Japan Agency for Marine-Earth Science and Technology, Atmosphere and Ocean Research Institute (The University of Tokyo), and National Institute for Environmental Studies	128 × 64, L80
MIROC-ESM-CHEM		128 × 64, L80
MRI-CGCM3	Meteorological Research Institute	320 × 160, L48
NorESM1-ME	Norwegian Climate Centre	144 × 96, L26
NorESM1-M		144 × 96, L26

future change (denoted as Δ) under global warming. The monthly outputs of precipitation, surface specific humidity, pressure velocity at the 500 hPa, and surface temperature, are used. We only select the first realization (r1i1p1) of each model. The MMM is calculated as the simple average of results from all models.

In terms of observations, the rainfall data are from the Global Precipitation Climatology Project (GPCP) dataset (Adler et al. 2003) and the Climate Prediction Center (CPC) Merged Analysis of Precipitation (CMAP) dataset (Xie and Arkin 1997). The pressure velocity is from the National Centers for Environmental Prediction–Department of Energy (NCEP–DOE) Atmospheric Model Intercomparison Project II reanalysis (Kanamitsu et al. 2002). The observations are selected for the period 1981–2000, which is the same as the historical run in CMIP5. The summer season in this study is defined as the average of June, July and August. All the model output and observational data are interpolated onto a 2.5° × 2.5° grid (from 90°S to 90°N, 0°E–357.5°E) using bilinear interpolation before analysis.

3 Methods

3.1 Moisture budget decomposition

To correct the projections of EASM rainfall changes (ΔP), we apply a simplified moisture budget decomposition (Huang et al. 2013) to divide the ΔP into two parts: the thermodynamic component and the dynamic component. Other relatively small terms, such as the changes in evaporation (ΔE), are omitted in this simplified decomposition (Zhou et al. 2018). This simplified moisture budget decomposition estimates the ΔP similarly to the complete moisture budget decomposition in Chou et al. (2009) in the EASM regions, therefore it is appropriate for the studies in the EASM regions (Zhou et al. 2018). It can be written as:

$$\Delta P = -\frac{1}{\rho_w g}(\Delta q \cdot \omega + q \cdot \Delta\omega) \quad (1)$$

where P is precipitation, q is the surface specific humidity and ω is the pressure velocity at 500 hPa. The ρ_w and g are

the density of water and standard gravity. The $-\Delta q \cdot \omega$ associated with the direct effect of moisture is the thermodynamic component, i.e. the component contributed by the "wet-get-wetter" mechanism (Chou and Neelin 2004; Held and Soden 2006), and the $-q \cdot \Delta\omega$ associated with circulation change is the dynamic component (Held and Soden 2006; Chou et al. 2009; Seager et al. 2010; Huang et al. 2013; Endo and Kitoh 2014). For simplicity, the constant coefficient $\frac{1}{\rho_w g}$ of Eq. (1) will be omitted in following study, but it still participates in the calculation.

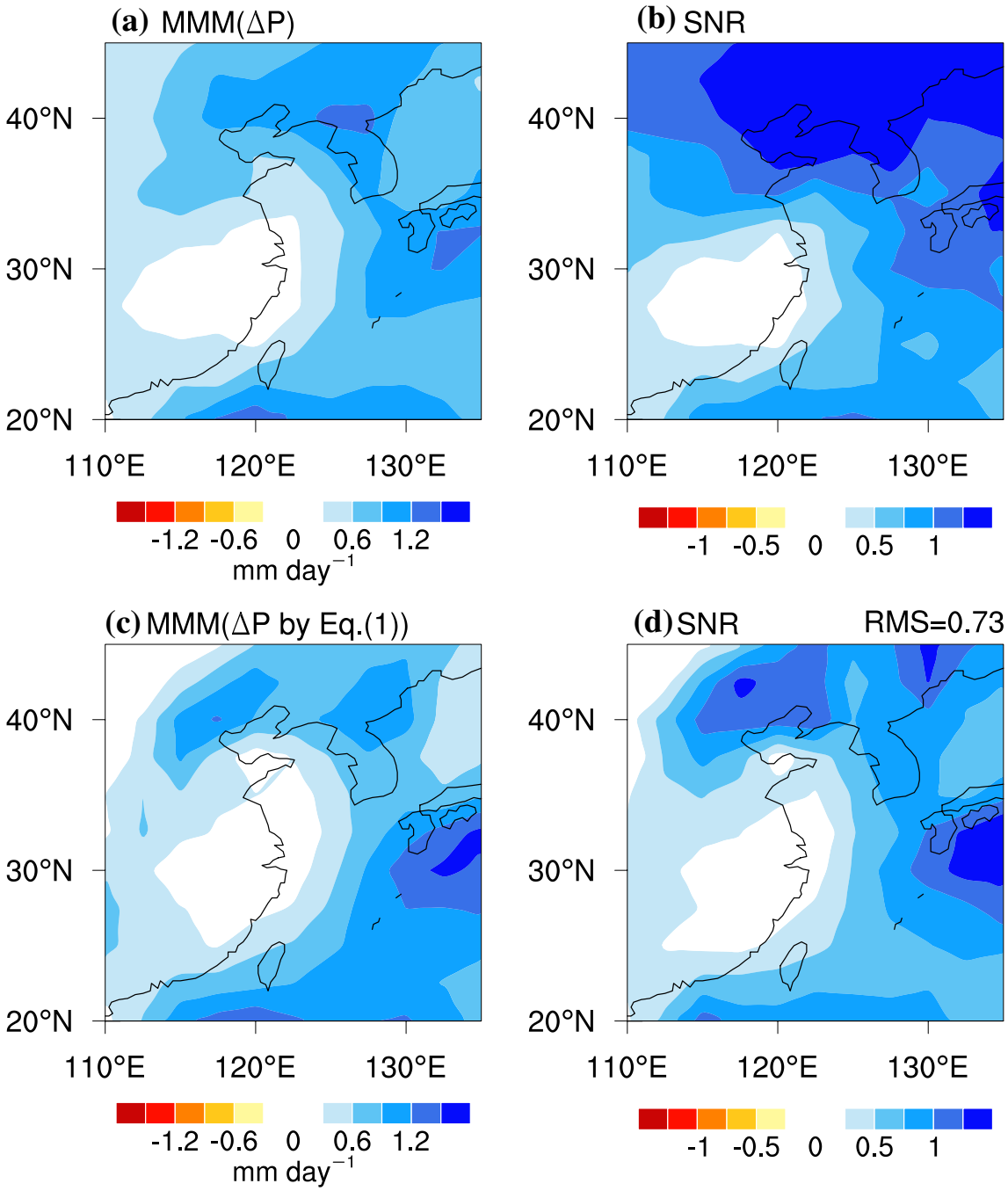

Fig. 1 **a** Multimodel mean (MMM) and **b** signal-to-noise (SNR) of the original summer-mean precipitation change (ΔP) of the 25 CMIP5 models under the RCP8.5 scenario, and **c** MMM and **d** SNR of the ΔP reconstructed by the thermodynamic and dynamic decomposition shown in Eq. (1). Root-mean-square (RMS) of the SNR of the ΔP is shown at the top-right corner of **(d)**

3.2 Correction for the thermodynamic component

According to the "wet-get-wetter mechanism" (Chou and Neelin 2004; Held and Soden 2006), the thermodynamic component of precipitation increases follow the rate of water vapor increase rate under global warming based on the Clausius–Clapeyron scaling. Here, we define a "thermodynamic constraint" to correct the thermodynamic component. The "thermodynamic constraint" method substitutes the thermodynamic component in Eq. (1) with $(\Delta q/q) \cdot P_{obs}$, where $\Delta q/q$ is the change rate of water vapor in each model basically following the Clausius–Clapeyron scaling (Chou and Neelin 2004; Held and Soden 2006) and P_{obs} is the present-day climatology of precipitation in the observation. Because rainfall datasets observed by satellites are more reliable than the available pressure velocity datasets. Therefore, we selected rainfall to replace pressure velocity in the correction for the thermodynamic component. The inconsistency between the pressure velocity at 500 hPa and rainfall mainly appears in climatological descending regions (Supplementary Material Fig. S1). As a result, the correction of thermodynamic component is feasible in the EASM region with adequate rainfall.

3.3 Correction for the dynamic component

For the dynamic component, we use an extended constraint strategy, the spatial emergent constraint (Huang and Ying 2015), to correct the circulation change ($\Delta\omega$; pressure velocity change at 500 hPa) within the dynamic component. The ensemble pattern regression method builds up historical-future relationships to estimate the common change bias that can then be used to correct the projection of future change (Huang and Ying 2015).

To validate the robustness for the dynamic correction, the perfect model approach is applied. The perfect model approach is also named leave-one-out cross validation, widely used in previous studies on emergent constraint projections (Räisänen et al. 2010; Abe et al. 2011; Bracegirdle and Stephenson 2012). This approach leaves out each of the 25 models in turn and treats it as a "perfect" target model. The historical variable (precipitation in this study) simulated in the target model is treated as the observation in the correction for the other 24 models, and the future change (pressure velocity change at 500 hPa in this study) projected by the target model is treated as a "perfectly" projected change in future to compare with the corrected results for the other models. We calculate the root mean square error (RMSE) between the projection corrected by the ensemble pattern regression and the "perfectly" projected change for each target model, and compare it with the RMSEs between the original MMM of the other 24 models before correction and the "perfectly" projected change in the target model to validate whether the spatial emergent constraint correction can make the multi-model projection closer to the "perfect" future changes.

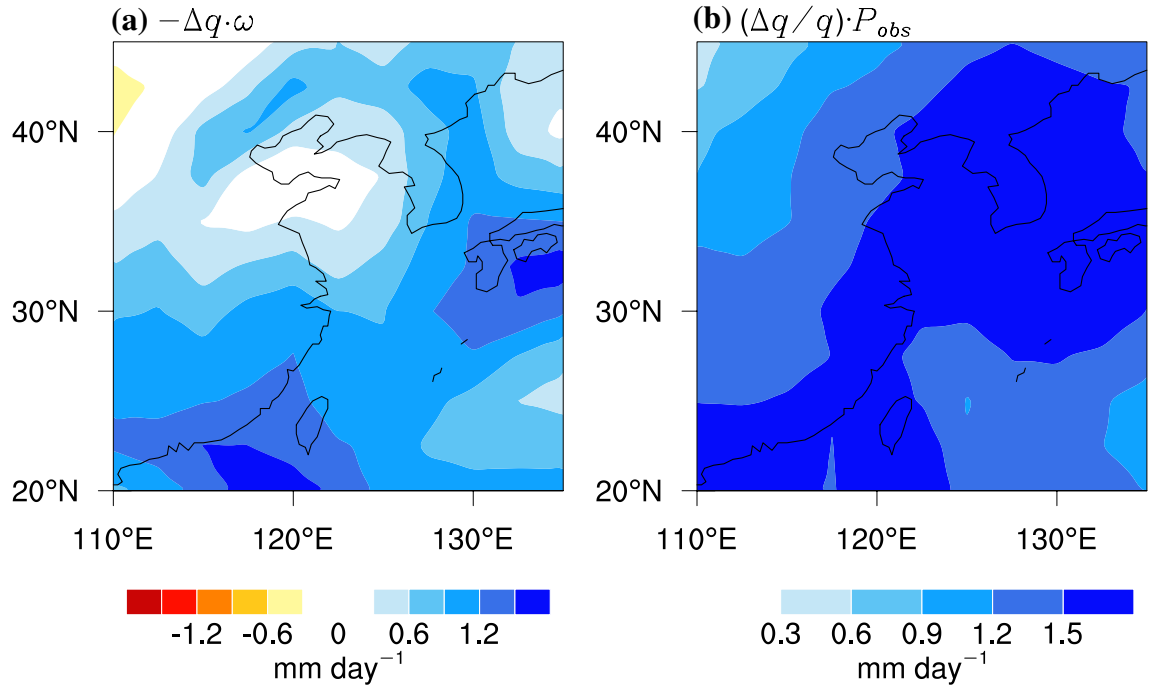

Fig. 2 MMM of **a** the thermodynamic component in ΔP of the 25 CMIP5 models and **b** MMM of $(\Delta q/q) \cdot P_{obs}$ used in the correction for the thermodynamic component

3.4 Metrics of intermodel uncertainty

In this study, the signal-to-noise ratio (SNR), defined as the ratio of multi-model mean and intermodel standard deviation of the 25 CMIP5 models, is applied to illustrate the robustness of the projection (e.g., Hu et al. 2003; Long et al. 2016; Huang 2017). To show the change of SNR more intuitive, the root-mean-square (RMS) of the SNR for all grids within the EASM regions is calculated to measure the effect of each correction step in the whole EASM domain.

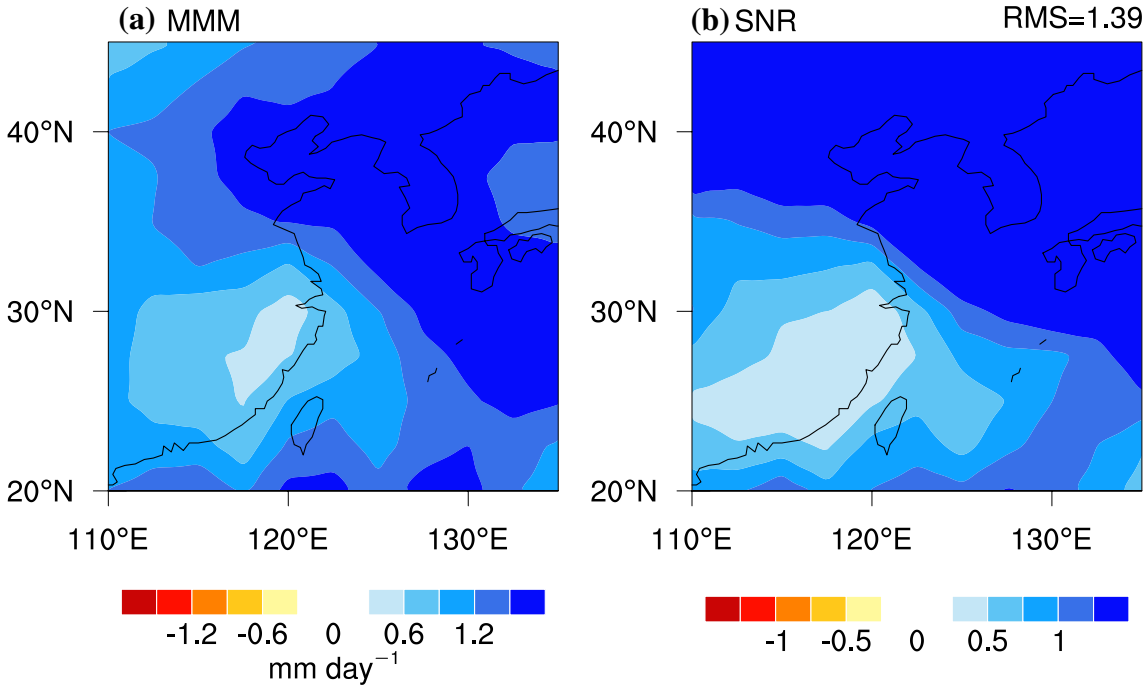

Fig. 3 **a** MMM and **b** SNR of summer-mean $[\Delta P]_{TH}$, the total rainfall changes with thermodynamic correction. RMS of the SNR of $[\Delta P]_{TH}$ is shown at the top-right corner of (**b**)

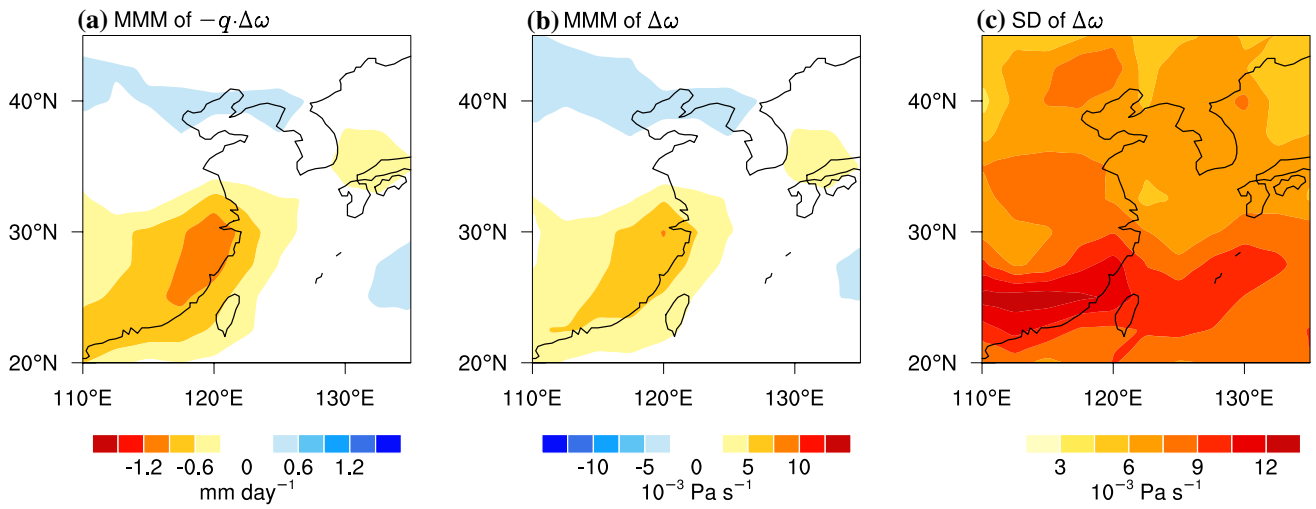

Fig. 4 MMM of **a** the dynamic component in ΔP of the 25 CMIP5 models, **b** MMM and **c** intermodel standard deviation of circulation change ($\Delta\omega$)

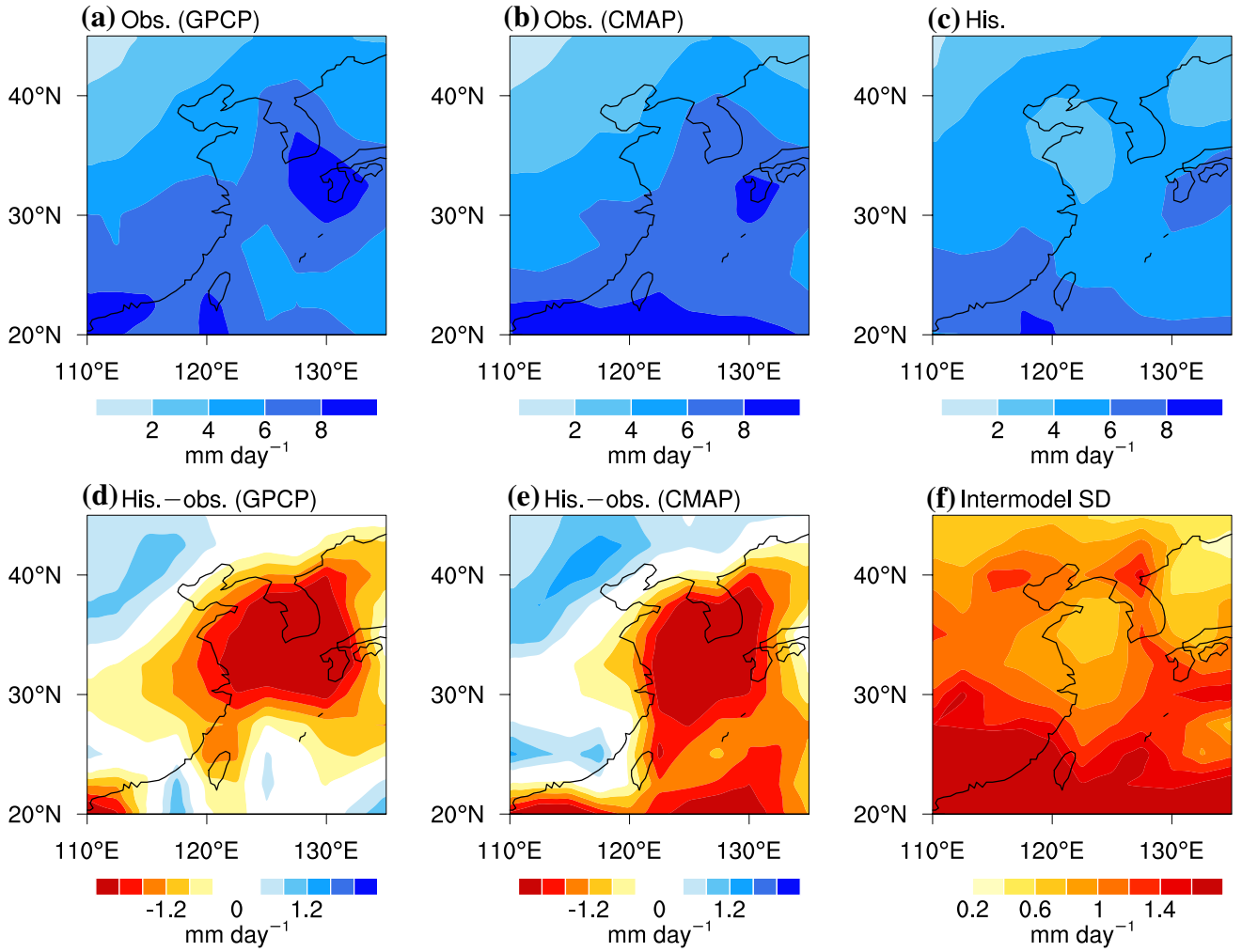

Fig. 5 **a** The observed (GPCP) summer-mean precipitation averaged from 1981 to 2000. **b** As in (**a**) but for CMAP. **c** MMM of the summer-mean precipitation of the 25 CMIP5 models in the historical run for 1981–2000. **d** Common historical bias in the precipitation relative to the observation (GPCP). **e** As in (**d**) but for CMAP. **f** Intermodel standard deviation of the historical summer-mean precipitation in the 25 CMIP5 models

4 Corrections

In order to distinguish the corrected ΔP, the ΔP with only thermodynamic correction is represented as $[\Delta P]_{TH}$, the ΔP with only dynamic correction is represented as $[\Delta P]_{DY}$, and the integrated correction of ΔP is written as $[\Delta P]_{TH+DY}$. Figure 1 shows the MMM and SNR of summer-mean ΔP (Fig. 1a, b) and the ΔP reconstructed by the thermodynamic and dynamic decomposition in Eq. (1) (Fig. 1c, d) in the EASM regions from the simulations of the 25 CMIP5 models. The projected ΔP (Fig. 1a) and ΔP calculated by moisture budget decomposition (Fig. 1c) are similar and exhibit an overall increase in the EASM regions (20°–45°N, 110°–135°E), except in mid-eastern China. Large intermodel spread leads to a low SNR in the EASM regions (Fig. 1b, d). The RMS of the SNR of EASM ΔP is only 0.73, suggesting quite low robustness in the EASM ΔP projected by the MMM of the CMIP5 models (Xie et al. 2015).

4.1 Correction for the thermodynamic component

The thermodynamic component $(-\Delta q \cdot \omega)$ of the moisture budget decomposition shows a positive effect on the EASM ΔP (Fig. 2a). Because the specific humidity changes (Δq) are positive in the EASM regions, the sign of thermodynamic component is primarily decided by the historical circulation (ω). Considerable intermodel spread exists in the ω of the 25 CMIP5 models, causing major uncertainty in the thermodynamic component (Zhou et al. 2018).

In this correction, we use $(\Delta q/q) \cdot P_{obs}$ to substitute the thermodynamic component, in which q is the historical specific humidity and P_{obs} is the present-day observed

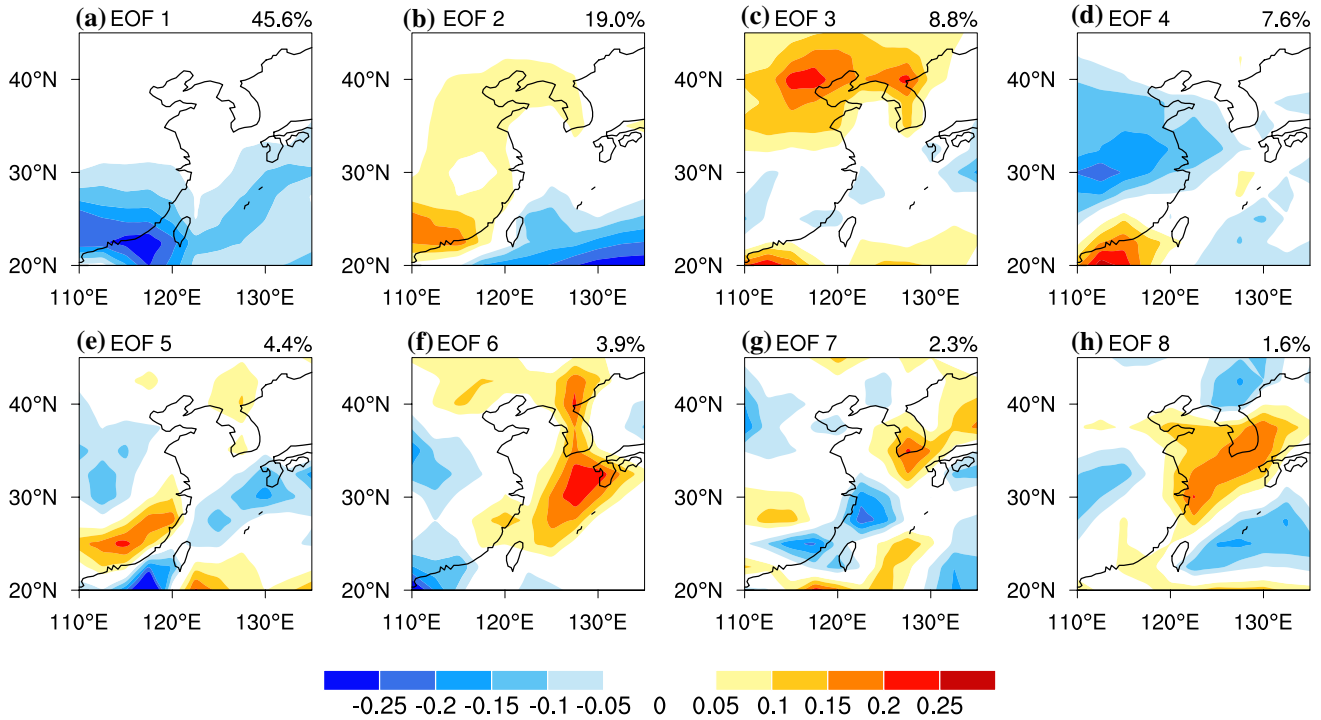

Fig. 6 Eight leading modes of the intermodel EOF for the individual historical bias of precipitation. The percentage of the variance explained by each mode is shown at the top-right corner of each panel

precipitation (GPCP used in this correction). The MMM of $(\Delta q/q) \cdot P_{obs}$ shows a maximum over the coastal region, the Yellow Sea and Japan (Fig. 2b). The $(\Delta q/q) \cdot P_{obs}$ is greater than the thermodynamic component represented by $-\Delta q \cdot \omega$ (Fig. 2a) possibly due to the widely underestimated EASM rainfall in the models.

We substitute the $-\Delta q \cdot \omega$ in the ΔP with $(\Delta q/q) \cdot P_{obs}$ and show the MMM and SNR of the $[\Delta P]_{TH}$ in Fig. 3. The maximum of $[\Delta P]_{TH}$ (Fig. 3a) locates over the northwest Pacific, Korea and northeast China, and the minimum over mid-eastern China, with a similar spatial pattern to the original ΔP (Fig. 1a). The SNR of $[\Delta P]_{TH}$ (Fig. 3b) prominently enhances in the EASM regions, and the RMS of the SNR of $[\Delta P]_{TH}$ reaches 1.39, which is much greater than that of the original ΔP (0.73; Fig. 1d).

4.2 Correction for the dynamic component

The main source of uncertainty in the dynamic component $(-q \cdot \Delta\omega)$ is the circulation change $(\Delta\omega)$ in the EASM regions (Zhou et al. 2018). We apply the spatial emergent constraint and the ensemble pattern regression method to correct the $\Delta\omega$, and then use the perfect model approach to validate the method used in the correction.

Figure 4 shows the MMM of dynamic component and $\Delta\omega$. The intermodel spread of $\Delta\omega$ (Fig. 4c) is larger than the MMM (Fig. 4b). Two sources of precipitation datasets, GPCP and CMAP, are chosen to show the dependence of the correction on observational datasets. The common historical bias of precipitation is the difference (Fig. 5d, e) between the observed precipitation (Fig. 5a, b) and the MMM precipitation in the historical run (Fig. 5c).

We apply an intermodel empirical orthogonal function (EOF) analysis to the individual historical rainfall biases of the 25 CMIP5 models. The eight leading EOF modes are shown in Fig. 6. The individual bias is the difference of a variable between the individual model and the MMM. The percentage of the variance explained by each mode is shown in the top-right corner of each panel, and these eight leading EOF modes together explain 93.2% of the variance. By projecting the common historical biases in the CMIP5 models onto these EOF modes, we obtain expansion coefficients for each mode (not shown) to reconstruct the common historical biases and estimate the possible bias in the projected changes induced by the background bias, which is also called the common change bias. Based on Figs. 6, 7b, e, the eight leading EOFs can capture well the spatial pattern of common historical biases by GPCP (Fig. 7e) in the region south of 35°N, but fail to achieve a good simulation in northern China, Korean Peninsula and Japan (Fig. 7e). We also show the reconstructions of the common historical biases by the first six and first ten EOF modes, along with the correlated residuals (Fig. 7). There are no differences between the reconstructions of the first eight and ten modes, implying

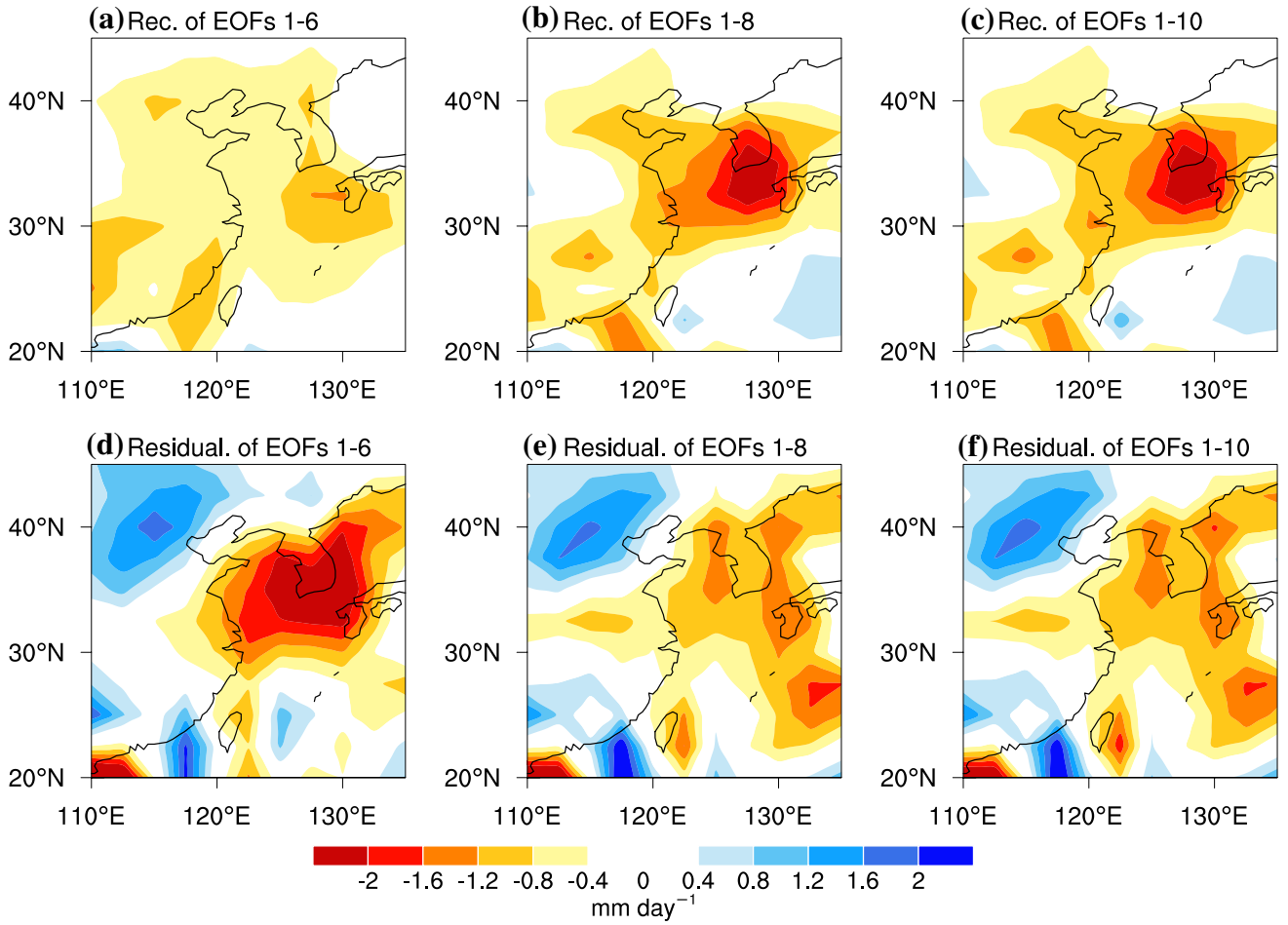

Fig. 7 Reconstruction of the common historical bias of precipitation by using the **a** six, **b** eight and **c** ten leading modes of the intermodel EOF analysis, and **d**–**f** the residual related to the reconstruction, with the observed data from GPCP

that the eight-mode truncation here is reasonable. The reconstruction based on the CMAP shown in the Supplementary Material (Fig. S2) is similar to the reconstruction by GPCP.

The next step is to build historical–future relationships to estimate the common change biases. The individual change biases of $\Delta\omega$ from the 25 CMIP5 models are regressed onto the PCs related with the EOF modes grid-by-grid, presenting the spatial structure of the regression coefficients in Fig. 8. The coefficients are scaled by the standard deviation of the corresponding PCs, and the explained variances of each regression are calculated to measure the contribution. All eight PCs explain about 46.7% of the total intermodel variance of the change bias. By combining the regression coefficients of the corresponding PCs with the expansion coefficients of the corresponding EOFs, we can obtain an estimation of the common change bias (Fig. 9a). Different observational data produce different expansion coefficients to influence the result of the estimation of the common change bias, which can also impact the correction. Comparing the correction results between the two sets of observations (Fig. 9b and Supplementary Material Fig. S3 for CMAP), the difference mainly locates in southern China. The intermodel uncertainty of $[\Delta\omega]_{DY}$ decreases by 15–45% relative to the uncertainty of $\Delta\omega$ (contours in Fig. 9c). Using different observational data does not influence the decrease of the uncertainty in $[\Delta\omega]_{DY}$, because the reduced uncertainty depends on the historical–future relationships. The results based on CMAP are shown in the Supplementary Material Fig. S3.

The perfect model approach is performed to validate the ensemble pattern regression method. Details of the perfect model approach are mentioned in Sect. 3.3. Figure 10 shows the ratio of RMSE by the dynamic correction to the RMSE before dynamic correction in the perfect model approach. A ratio under 100% indicates the improvement by ensemble pattern regression method. The reduction of the RMSE almost covers all the EASM region except the Yellow Sea. This result suggests that the ensemble pattern regression method used in the dynamic correction can improve the robustness of the 500-hPa pressure velocity change in simulation.

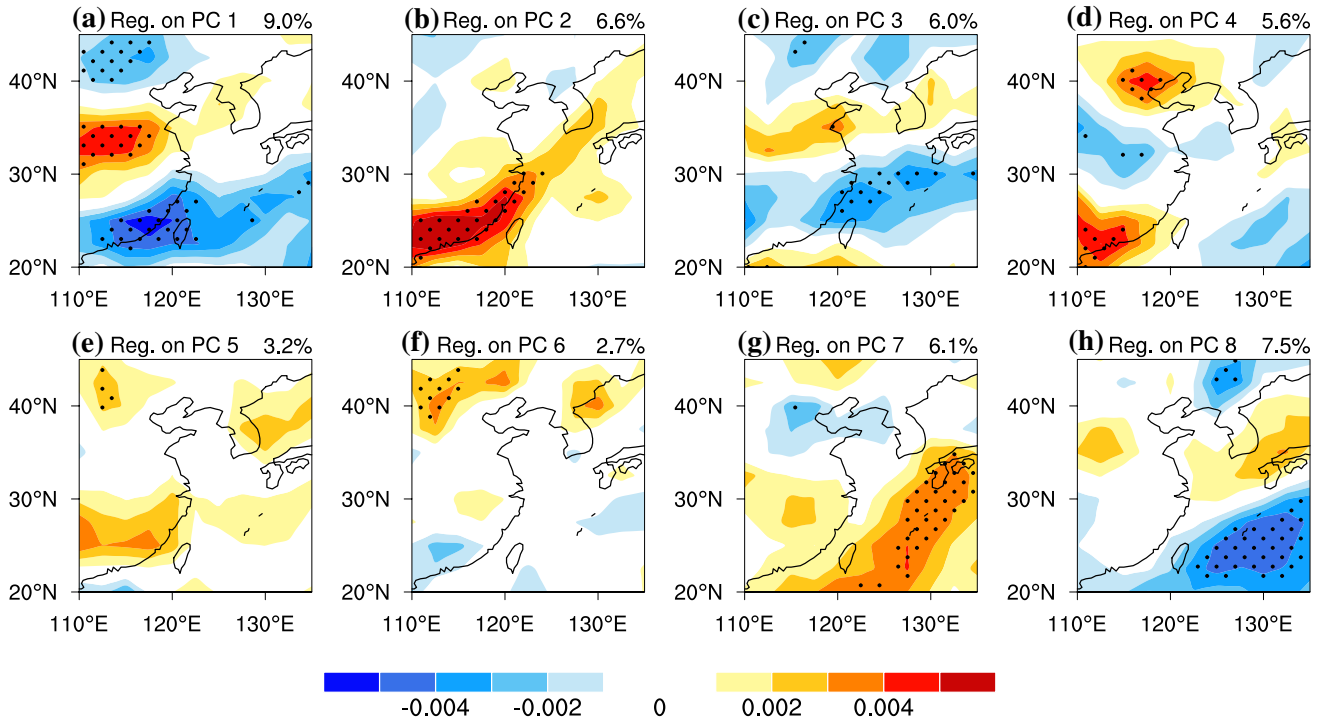

Fig. 8 Regression pattern of $\Delta\omega$ onto the PCs associated with the intermodal EOF modes shown in Fig. 6. Each regression pattern is scaled by the standard deviation of the corresponding PC. The percentage of the variance explained by each PC is shown at the top-right corner of each panel. Stippling indicates where the regression passes the *t* test at the 95% significance level

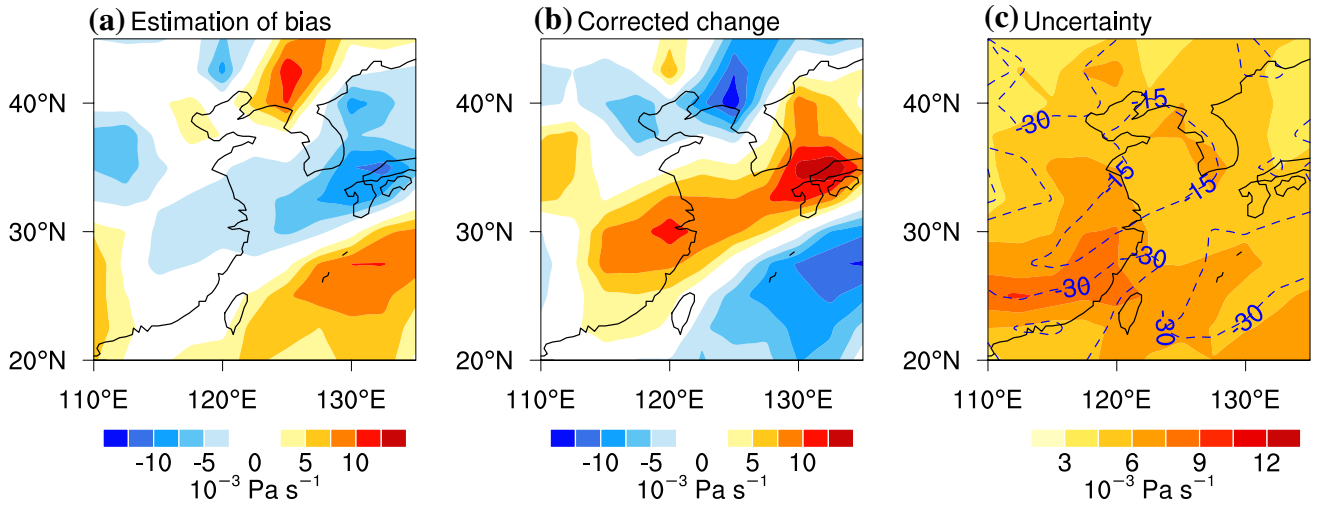

Fig. 9 **a** Estimated common change bias of $\Delta\omega$. **b** Corrected MMM of $\Delta\omega$. **c** Intermodel standard deviation (shaded) of $[\Delta\omega]_{DY}$ and the percentage change (contours; contour interval is 15% and negative contours are dashed) relative to the $\Delta\omega$, with the observed data from GPCP

4.3 Integrated projection

Finally, we put $[\Delta\omega]_{DY}$ back into Eq. (1) and show the MMM and SNR of $[\Delta P]_{DY}$ in Fig. 11 and in the Supplementary Material Fig. S4 for CMAP. The RMS of the SNR of $[\Delta P]_{DY}$ increasing by around 64% indicates that the ensemble pattern regression method can improve the robustness of the projected rainfall change. We further present the integrated correction of rainfall change ($[\Delta P]_{TH+DY}$; Fig. 12 and Supplementary Material Fig. S5 for CMAP). There is a 160% increase in the RMS of the SNR for ΔP, which indicates that this integrated correction method can provide a more

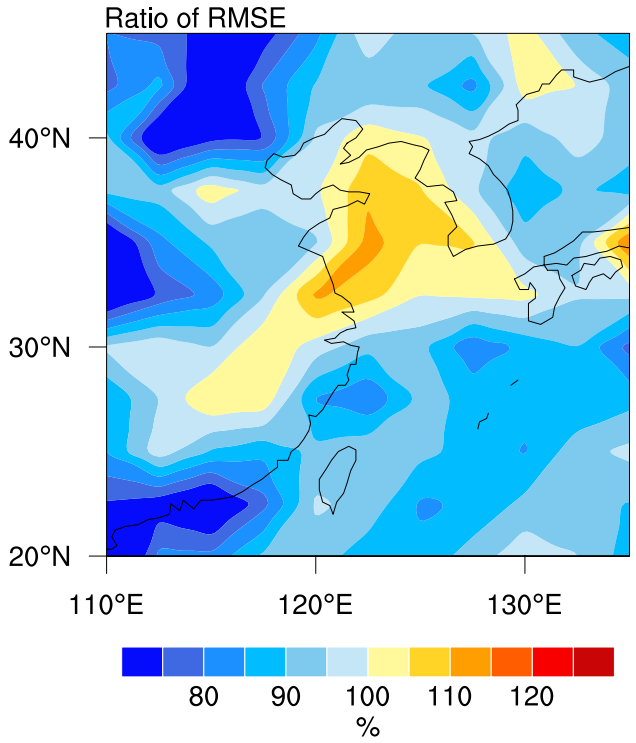

Fig. 10 Ratio of root mean square error (RMSE) by the dynamic correction to the RMSE before dynamic correction in the perfect model approach. The RMSE is integrated for all 25 models

robust projection of the EASM rainfall change. In addition, we calculated the RMS of the thermodynamic and dynamic components to compare their contributions to the rainfall changes. Before correction, the RMSs of the thermodynamic and dynamic components in EASM region are 0.91 and 0.4 mm day^{-1} with their ratio of 2.3, and after correction the RMSs of the thermodynamic and dynamic components are 1.53 and 0.9 mm day^{-1} with a decreased ratio of 1.7. The thermodynamic component still dominates the rainfall changes in EASM region.

The integrated projection of the EASM ΔP shows a pronounced enhancement in southern China, the northwest Pacific and a belt extending from northern China, to the Korean Peninsula and northeastern China, and a weak enhancement in the other EASM regions. Especially noteworthy is that the changes over the Yangtze River Valley corrected with GPCP are distinct from those corrected with CMAP, with the former remaining almost constant but the latter yielding a weak increase. This result suggests that the choice of "observation" could be another source of uncertainty in these corrected projections.

4.4 Projections under global warming of 1.5 °C and 2 °C

Figure 13 depicts the MMM of $[\Delta P]_{TH+DY}$ for global warming of 1.5 °C and 2 °C, which are derived by linearly scaling $[\Delta P]_{TH+DY}$ with respective warming rates. Under global

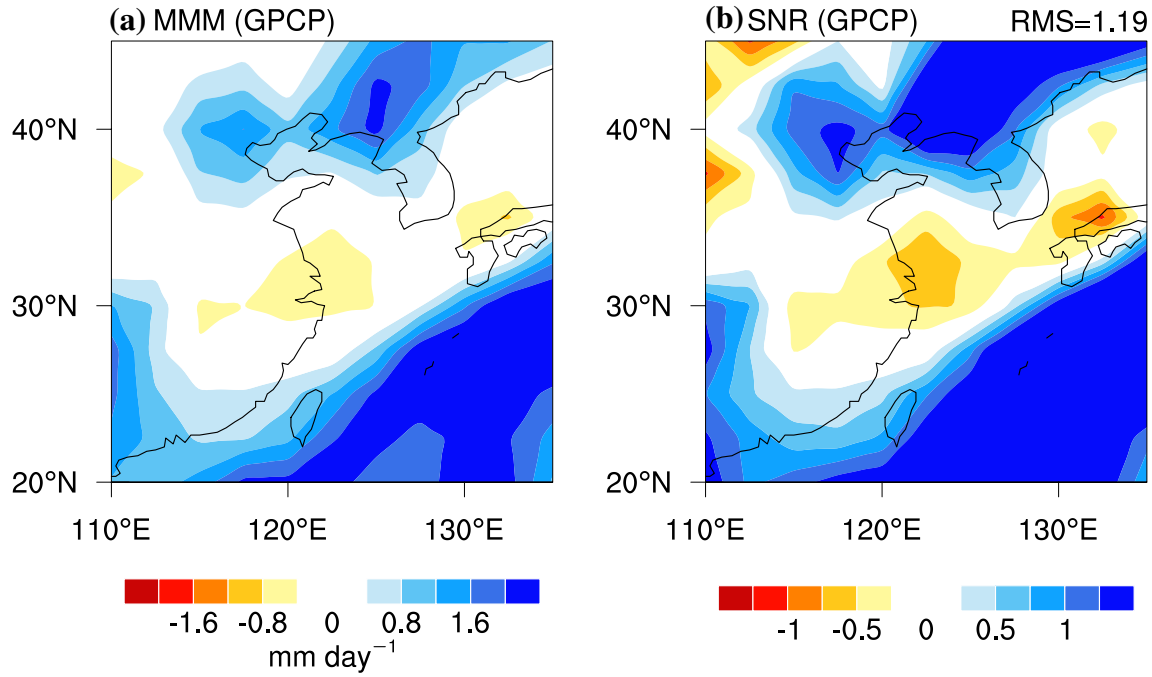

Fig. 11 **a** MMM and **b** SNR of the summer-mean $[\Delta P]_{DY}$, the total rainfall changes with only dynamic correction by GPCP rainfall datasets. RMS of the SNR of $[\Delta P]_{DY}$ is shown at the top-right corner of (**b**)

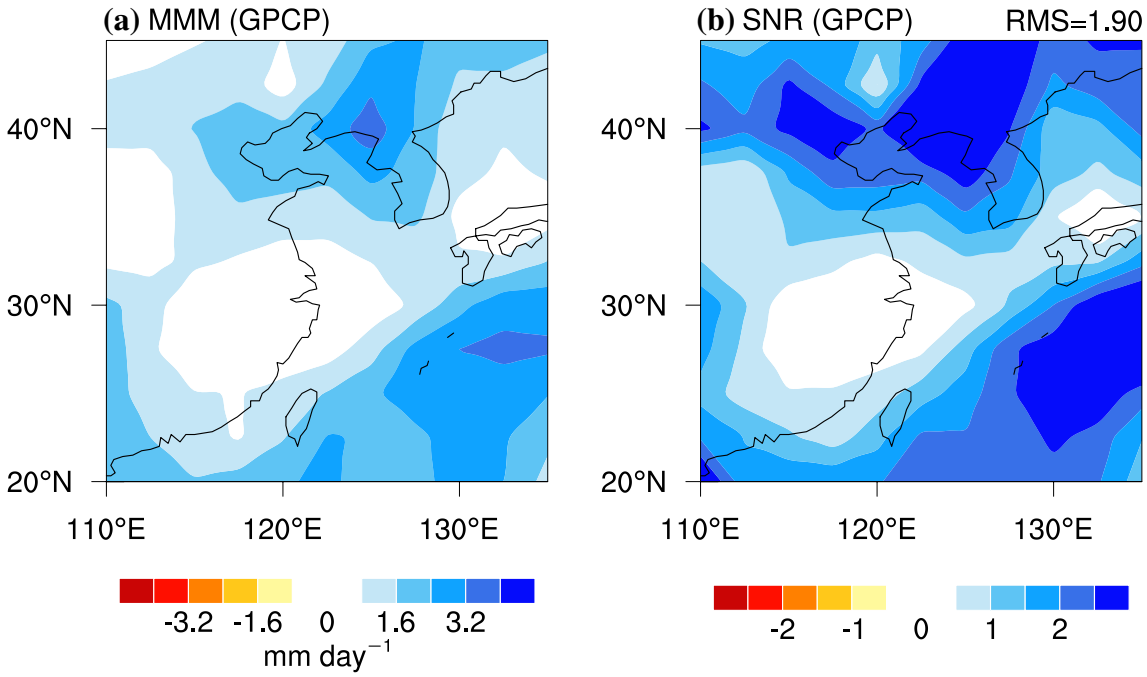

Fig. 12 **a** MMM and **b** SNR of the summer-mean $[\Delta P]_{TH+DY}$, with both the thermodynamic correction and the dynamic correction. The color bars in this figure are twice those in Fig. 11

warming of 1.5 °C (Fig. 13a, c), EASM rainfall increases by around 5–15% in the northwest Pacific and the belt from northern China to northeastern China, and by less than 5% in the other regions, relative to present-day precipitation. And under global warming of 2 °C global (Fig. 13b, d), the increase is around 10–25% in the northwest Pacific and the belt from northern China to northeastern China, and 5–10% in the other EASM regions. We also find that the changes in the Yangtze River Valley are distinct between the projections using the GPCP and CMAP. The Yangtze River Valley rainfall is projected to increase by around 5% and 5–10% under global warming of 1.5 °C and 2 °C, respectively, when the correction is based on CMAP; whereas, when based on GPCP, rainfall in this region remains constant under 1.5 °C warming and increases only by around 5% under a warming of 2 °C.

5 Conclusions and discussion

The low reliability of climate model projections of EASM rainfall changes is an important issue for regional climate change under global warming. Large intermodel uncertainty exists in the projection of EASM rainfall changes among the CMIP5 models. As a conventional method to provide an average result from all climate models, the MMM seems unconvincing when the climate change signals are smaller than the intermodel spread. In the present study, we introduce a bias-corrected method to correct the MMM projection for the EASM rainfall changes based on 25 CMIP5 models. The integrated projection includes two steps: (1) correction by Clausius–Clapeyron scaling for the thermodynamic component; and (2) a spatial emergent constraint correction for the dynamic component.

Firstly, the Clausius–Clapeyron scaling correction improves the robustness of the EASM ΔP projections, with the RMS of the SNR increasing to 1.39 from the original 0.73. Further, we use a spatial emergent constraint with the ensemble pattern regression method in Huang and Ying (2015) with two sets of observational precipitation data to correct the $\Delta\omega$ in the dynamic component. In the ensemble pattern regression correction, the possible bias in the projected $\Delta\omega$ induced by the background bias is estimated based on the intermodal spread of the $\Delta\omega$ and the historical precipitation, and then used to correct the MMM of the $\Delta\omega$. To validate the method used in the dynamic correction, we apply the perfect model approach. The results suggest that the dynamic correction can provide a more robust projection of the future pressure velocity change. Finally, all the corrections integrated together increase the regional RMS of the SNR of the EASM ΔP to around 1.9 from the 0.73 of the original ΔP, which is an increase of about 160%. This improvement suggest that this bias-corrected method can enhance the robustness of projected EASM rainfall changes under global warming. The corrected EASM rainfall changes show a pronounced enhancement in southern

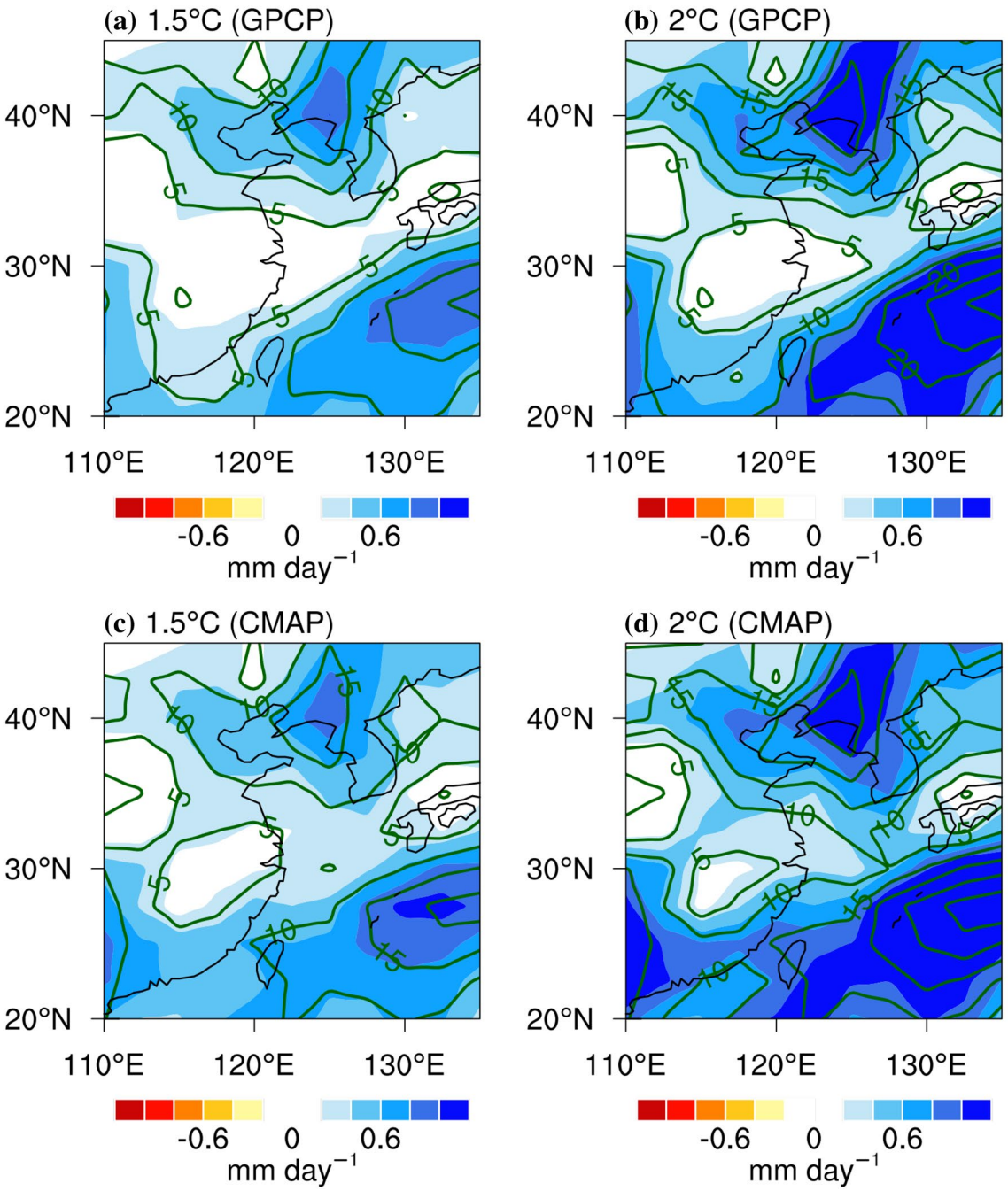

Fig. 13 MMM of $[\Delta P]_{TH+DY}$ under global warming of **a**, **c** 1.5 °C and **b**, **d** 2 °C, based on GPCP and CMAP data. Contours are the percentage change for $[\Delta P]_{TH+DY}$ relative to the historical (1981–2000) climatology of rainfall

China, the northwest Pacific and a belt from northern China to the Korean Peninsula and northeastern China, and a weak enhancement in the other EASM regions.

To show a bias-corrected projection under global warming of 1.5 °C and 2 °C, we linearly scaled the corrected EASM ΔP to global warming of 1.5 °C and 2 °C, i.e., the goal of the Paris Agreement. Under 1.5 °C warming, the EASM ΔP might increase by 5–15% in the northwest Pacific and the belt from northern China to northeastern China, and by less than 5% in the other regions, relative to the present-day precipitation. And under 2 °C warming, the EASM ΔP increases by around 10–25% in the

northwest Pacific and the belt from northern China to northeastern China, and by 5–10% in the other EASM regions. We also find that the changes in the Yangtze River Valley are distinct between projections using different observational data.

Based on a simplified moisture budget decomposition [Eq. (1)] to study the EASM rainfall change, we neglect the residuals in Eq. (1). The residuals can be calculated as the difference between Fig. 1a, c, and the effects of the correction can be calculated as the difference between Figs. 1c, 12a. We compare the residuals to the correction change in Supplementary Material Fig. S6. The residuals are much weaker than the correction change, suggesting that the residuals provide little influence on the correction results in this study.

In addition to the selection of different observation dataset, the selection of historical variable is also crucial. We empirically selected precipitation as historical variable used in the ensemble pattern regression method to correct the dynamic component. However, some other factors, such as the western North Pacific subtropical high and the pattern of sea surface warming, may also influence the EASM circulation and rainfall changes (Chen and Zhou 2015; He and Zhou 2015). In a recent study, Li et al. (2017) found that models simulating excessive historical rainfall over the tropical western Pacific project larger increase in Indian summer monsoon rainfall under global warming. Excessive rainfall leads to strong negative cloud–radiation feedback and suppresses sea surface warming, changing the atmospheric circulation (Gill 1980). Other studies have also revealed that certain climatological biases in models can impact projections of future climate changes in the tropics (Zhou and Xie 2015; Ying and Huang 2016; Ham et al. 2018). In the subtropics, both the tropical and mid-latitude climate systems can affect the EASM, which is a more complicated picture than in the tropics. The potential factors and underlying mechanism associated with intermodel uncertainty in EASM rainfall changes and circulation changes need further study in the future.

Acknowledgements This work is supported by the National Natural Science Foundation of China (41575088, 41722504, 41425019, 41721004 and 41661144016), the Strategic Priority Research Program of Chinese Academy of Sciences (XDA20060501), the Public Science and Technology Research Funds Projects of Ocean (201505013), and the Youth Innovation Promotion Association of CAS and the Fundamental Research Funds for the Central Universities. We acknowledge the World Climate Research Programme's Working Group on Coupled Modeling, which is responsible for CMIP5, and the climate modeling groups (listed in Table 1) for producing and making available their model output. We also thank two anonymous reviewers for their constructive suggestions.

Appendix: Spatial emergent constraint and Ensemble pattern regression method

The spatial emergent constraint with the ensemble pattern regression method used in this study was first developed in Huang and Ying (2015), extending the original emergent constraint for regional-mean changes, to constrain the future changes with apparent spatial pattern. The main steps are introduced here.

We indicate the historical climatology of model i by H_i and the future climatology by F_i. The future change C_i is defined as $C_i = F_i - H_i$. We suppose that there is a perfect projection of future change C_{real}, which is the same in all models, and the difference between the C_{real} and the MMM change $\bar{C} = N^{-1}\sum_{i=1}^{N} C_i$ is the common change bias $\bar{C}' = \bar{C} - C_{real}$. For the individual change bias C_i'', this is defined as $C_i'' = C_i - \bar{C}$ and the total change bias of a model i is $C_i' = \bar{C}' + C_i''$. An identical decomposition method can be applied to the H_i. The historical climatology H_i consists of the observed climatology H_{obs}, the common historical bias $\bar{H}' = N^{-1}\sum_{i=1}^{N} H_i - H_{obs}$ and the individual historical bias $H_i'' = H_i - \bar{H}$.

Next, we need to build up the spatially correlated mode between the historical bias and the change bias. EOF analysis is a common method to decompose a signal into a time series and spatial pattern. However, here we apply an intermodel EOF analysis to the H_i'' of all the model and get the spatially orthogonal modes EOF_j, $j = 1, \ldots, M$ and corresponding principal coefficients PC_{ij}. For a specific H_i'', this can be represented as $H_i'' = \sum_{j=1}^{M} \mathrm{EOF}_j \mathrm{PC}_{ij}$. The truncation of M EOFs depends on the representation of the EOF modes for the historical bias H_i'' and $\bar{H}'$, and influences the results of the correction. Multivariant linear regression analysis is performed on PCs and individual change bias C''. The estimation of C'' can be calculated by the regression pattern $\hat{b}$ and PCs:

$$\hat{C}_i'' = \sum_{j=1}^{M} \hat{b}_j \mathrm{PC}_{ij}. \tag{2}$$

Because the PCs are linearly independent, the regression pattern $\hat{b}$ equals the simple linear regression result of C'' onto PCs mode by mode. This simplifies the procedure of regression.

The estimation of the common change bias $\bar{C}'$ is based on a hypothesis that the relationship between $\bar{C}'$ and the common historical bias $\bar{H}'$ is the same as the relationship between the modes of EOF_j and $\hat{b}_j$. First, we project the $\bar{H}'$ onto EOF_j and represent the $\bar{H}'$ by the expansion coefficient e_j:

$$\bar{H}' = \sum_{j=1}^{M} \mathrm{EOF}_j e_j. \tag{3}$$

We replace the PCs in Eq. (2) by the expansion coefficient e_j and estimate $\bar{C}'$:

$$\hat{\bar{C}}' = \sum_{j=1}^{M} \hat{b}_j e_j. \tag{4}$$

Finally, we can correct the MMM change $\bar{C}$ as $\bar{C}_C = \bar{C} - \hat{\bar{C}}'$. The individual change in model i C_i can also be corrected as the correction for common bias in MMM. We then just need to substitute the common historical bias $\bar{H}'$ in Eq. (3) with the total historical bias $H_i^{'} = H_i - H_{obs}$:

$$H_i^{'} = \sum_{j=1}^{M} \mathrm{EOF}_j e_{ij}. \tag{5}$$

The expansion coefficient e_{ij} for H_i' can replace the e_j in Eq. (4):

$$\hat{C}_i' = \sum_{j=1}^{M} \hat{b}_j e_{ij}. \tag{6}$$

The individual change in model i is corrected as $C_{Ci} = C_i - \hat{C}_i'$.

References

Abe M, Shiogama H, Nozawa T, Emori S (2011) Estimation of future surface temperature changes constrained using the future-present correlated modes in inter-model variability of CMIP3 multimodel simulations. J Geophys Res 116:D18104

Adler RF, Huffman GJ, Chang A, Ferraro R, Xie P-P, Janowiak J, Rudolf B, Schneider U, Curtis S, Bolvin D, Gruber A, Susskind J, Arkin P, Nelkin E (2003) The version-2 global precipitation climatology project (GPCP) monthly precipitation analysis (1979–present). J Hydrometeorol 4(6):1147–1167

Allen MR, Ingram WJ (2002) Constraints on future changes in climate and the hydrologic cycle. Nature 419(6903):224–232

Bracegirdle TJ, Stephenson DB (2012) Higher precision estimates of regional polar warming by ensemble regression of climate model projections. Climate Dyn 39(12):2805–2821

Bracegirdle TJ, Stephenson DB (2013) On the robustness of emergent constraints used in multimodel climate change projections of arctic warming. J Climate 26(2):669–678

Brown JR, Moise AF, Colman R, Zhang H (2016) Will a warmer world mean a wetter or drier Australian monsoon? J Climate 29(12):4577–4596

Byrne MP, O'Gorman PA (2015) The response of precipitation minus evapotranspiration to climate warming: why the "wet-get-wetter, dry-get-drier" scaling does not hold over land. J Climate 28(20):8078–8092

Byrne MP, O'Gorman PA (2013) Link between land-ocean warming contrast and surface relative humidities in simulations with coupled climate models. Geophys Res Lett 40(19):5223–5227

Chen H, Sun J (2013) Projected change in East Asian summer monsoon precipitation under RCP scenario. Meteorol Atmos Phys 121(1–2):55–77

Chen X, Zhou T (2015) Distinct effects of global mean warming and regional sea surface warming pattern on projected uncertainty in the South Asian summer monsoon. Geophys Res Lett 42(21):9433–9439

Chou C, Neelin JD (2004) Mechanisms of global warming impacts on regional tropical precipitation. J Climate 17:2688–2701

Chou C, Neelin JD, Chen C-A, Tu J-Y (2009) Evaluating the "rich-get-richer" mechanism in tropical precipitation change under global warming. J Climate 22(8):1982–2005

Chou C, Chiang JCH, Lan C-W, Chung C-H, Liao Y-C, Lee C-J (2013) Increase in the range between wet and dry season precipitation. Nat Geosci 6(4):263–267

Collins M, Chandler RE, Cox PM, Huthnance JM, Rougier J, Stephenson DB (2012) Quantifying future climate change. Nat Climate Change 2(6):403–409

Cox PM, Pearson D, Booth BB, Friedlingstein P, Huntingford C, Jones CD, Luke CM (2013) Sensitivity of tropical carbon to climate change constrained by carbon dioxide variability. Nature 494:341

de Carvalho LMV (2016) The monsoons and climate change. In: de Carvalho LMV, Jones C (eds) The monsoons and climate change: observations and modeling. Springer International Publishing, Berlin

Ding Y, Chan JCL (2005) The East Asian summer monsoon: an overview. Meteorol Atmos Phys 89:117–142

Endo H, Kitoh A (2014) Thermodynamic and dynamic effects on regional monsoon rainfall changes in a warmer climate. Geophys Res Lett 41(5):1704–1711

Gao Y, Wang H, Jiang D (2015) An intercomparison of CMIP5 and CMIP3 models for interannual variability of summer precipitation in Pan-Asian monsoon region. Int J Climatol 35(13):3770–3780

Gill AE (1980) Some simple solutions for heat-induced tropical circulation. Q J R Meteorol Soc 106(449):447–462

Hall A, Cox P, Huntingford C, Klein S (2019) Progressing emergent constraints on future climate change. Nat Climate Change 9(4):269–278

Ham Y-G, Kug J-S, Choi J-Y, Jin F-F, Watanabe M (2018) Inverse relationship between present-day tropical precipitation and its sensitivity to greenhouse warming. Nat Climate Change 8(1):64–69

Hawkins E, Sutton R (2009) The potential to narrow uncertainty in regional climate predictions. Bull Am Meteorol Soc 90(8):1095–1107

Hawkins E, Sutton R (2011) The potential to narrow uncertainty in projections of regional precipitation change. Climate Dyn 37(1–2):407–418

He C, Zhou T (2015) Responses of the Western North Pacific subtropical high to global warming under RCP4.5 and RCP8.5 scenarios projected by 33 CMIP5 models: the dominance of tropical Indian Ocean–tropical Western Pacific SST gradient. J Climate 28(1):365–380

Held IM, Soden BJ (2006) Robust responses of the hydrological cycle to global warming. J Climate 19:5686–5699

Hsu P-c, Li T, Luo J-J, Murakami H, Kitoh A, Zhao M (2012) Increase of global monsoon area and precipitation under global warming: a robust signal? Geophys Res Lett 39(6):L06701

Hu Z-Z, Yang S, Wu R (2003) Long-term climate variations in China and global warming signals. J Geophys Res 108(19):4614

Huang P (2014) Regional response of annual-mean tropical rainfall to global warming. Atmos Sci Lett 15(2):103–109

Huang P (2017) Time-varying response of ENSO-induced tropical pacific rainfall to global warming in CMIP5 models. Part II: intermodel uncertainty. J Climate 30(2):595–608

Huang P, Ying J (2015) A multimodel ensemble pattern regression method to correct the tropical Pacific SST change patterns under global warming. J Clim 28(12):4706–4723

Huang P, Xie S-P, Hu K, Huang G, Huang R (2013) Patterns of the seasonal response of tropical rainfall to global warming. Nat Geosci 6(5):357–361

Kanamitsu M, Ebisuzaki W, Woollen J, Yang S-K, Hnilo JJ, Fiorino M, Potter GL (2002) NCEP–DOE AMIP-II reanalysis (R-2). Bull Am Meteorol Soc 83(11):1631–1644

Kent C, Chadwick R, Rowell DP (2015) Understanding uncertainties in future projections of seasonal tropical precipitation. J Climate 28(11):4390–4413

Kimoto M (2005) Simulated change of the East Asian circulation under global warming scenario. Geophys Res Lett 32:L16701

Kitoh A, Endo H, Krishna Kumar K, Cavalcanti IFA, Goswami P, Zhou T (2013) Monsoons in a changing world: a regional perspective in a global context. J Geophys Res Atmos 118(8):3053–3065

Klein SA, Hall A (2015) Emergent constraints for cloud feedbacks. Curr Climate Change Rep 1(4):276–287

Knutti R (2010) The end of model democracy? Climate Change 102(3–4):395–404

Kusunoki S, Mizuta R (2013) Changes in precipitation intensity over East Asia during the 20th and 21st centuries simulated by a global atmospheric model with a 60 km grid size. J Geophys Res Atmos 118(19):11007–11016

Li X, Ting M (2017) Understanding the Asian summer monsoon response to greenhouse warming: the relative roles of direct radiative forcing and sea surface temperature change. Climate Dyn 49(7–8):2863–2880

Li G, Xie S-P (2014) Tropical biases in CMIP5 multimodel ensemble: the excessive Equatorial Pacific cold tongue and double ITCZ problems. J Climate 27(4):1765–1780

Li G, Xie S-P, He C, Chen Z (2017) Western Pacific emergent constraint lowers projected increase in Indian summer monsoon rainfall. Nat Climate Change 7(10):708–712

Long S-M, Xie S-P, Liu W (2016) Uncertainty in tropical rainfall projections: atmospheric circulation effect and the ocean coupling. J Climate 29(7):2671–2687

Mike H, Zhao Z-C, Jiang T (1994) Recent and future climate change in East Asia. Int J Climatol 14:637–658

Räisänen J, Ruokolainen L, Ylhäisi J (2010) Weighting of model results for improving best estimates of climate change. Climate Dyn 35(2–3):407–422

Roderick ML, Sun F, Lim WH, Farquhar GD (2014) A general framework for understanding the response of the water cycle to global warming over land and ocean. Hydrol Earth Syst Sci 18(5):1575–1589

Seager R, Naik N, Vecchi GA (2010) Thermodynamic and dynamic mechanisms for large-scale changes in the hydrological cycle in response to global warming. J Climate 23(17):4651–4668

Seo KH, Ok J, Son JH, Cha DH (2013) Assessing future changes in the East Asian Summer Monsoon using CMIP5 coupled models. J Climate 26(19):7662–7675

Song F, Zhou T (2014) The climatology and interannual variability of East Asian Summer Monsoon in CMIP5 coupled models: does air-sea coupling improve the simulations? J Climate 27(23):8761–8777

Sperber KR, Annamalai H, Kang IS, Kitoh A, Moise A, Turner A, Wang B, Zhou T (2013) The Asian summer monsoon: an intercomparison of CMIP5 vs. CMIP3 simulations of the late 20th century. Climate Dyn 41(9–10):2711–2744

Thomson MC, Doblas-Reyes FJ, Mason SJ, Hagedorn R, Connor SJ, Phindela T, Morse AP, Palmer TN (2006) Malaria early warnings based on seasonal climate forecasts from multi-model ensembles. Nature 439(7076):576–579

Ueda H, Iwai A, Kuwako K, Hori ME (2006) Impact of anthropogenic forcing on the Asian summer monsoon as simulated by eight GCMs. Geophys Res Lett 33(6):L06703

Vecchi GA, Soden BJ, Wittenberg AT, Held IM, Leetmaa A, Harrison MJ (2006) Weakening of tropical Pacific atmospheric circulation due to anthropogenic forcing. Nature 441(7089):73–76

Wang B, Yim S-Y, Lee J-Y, Liu J, Ha K-J (2014) Future change of Asian-Australian monsoon under RCP 4.5 anthropogenic warming scenario. Climate Dyn 42(1–2):83–100

Wu P, Christidis N, Stott P (2013) Anthropogenic impact on Earth's hydrological cycle. Nat Climate Change 3(9):807–810

Xie P, Arkin PA (1997) Global precipitation: a 17-year monthly analysis based on gauge observations, satellite estimates, and numerical model outputs. Bull Am Meteorol Soc 78(11):2539–2558

Xie S-P, Deser C, Vecchi GA, Ma J, Teng H, Wittenberg AT (2010) Global warming pattern formation: sea surface temperature and rainfall. J Climate 23(4):966–986

Xie S-P, Deser C, Vecchi GA, Collins M, Delworth TL, Hall A, Hawkins E, Johnson NC, Cassou C, Giannini A, Watanabe M (2015) Towards predictive understanding of regional climate change. Nat Climate Change 5(10):921–930

Ying J, Huang P (2016) Cloud-radiation feedback as a leading source of uncertainty in the tropical pacific SST warming pattern in CMIP5 models. J Climate 29(10):3867–3881

Zheng Y, Shinoda T, Lin J-L, Kiladis GN (2011) Sea surface temperature biases under the stratus cloud deck in the Southeast Pacific Ocean in 19 IPCC AR4 coupled general circulation models. J Climate 24(15):4139–4164

Zhou Z-Q, Xie S-P (2015) Effects of climatological model biases on the projection of tropical climate change. J Climate 28(24):9909–9917

Zhou S, Huang G, Huang P (2018) Changes in the East Asian summer monsoon rainfall under global warming: moisture budget decompositions and the sources of uncertainty. Climate Dyn 51(4):1363–1373